Redundancy resolution and control of manipulators driven by antagonistic pneumatic muscles

Mauro Calabria, Frank Schreiber, Yevgen Sklyarenko, David Inkermann,
Annika Raatz, Thomas Vietor and Walter Schumacher

***Abstract*— Pneumatic artificial muscles feature lightweight and compact design, in combination with high obtainable forces and an intrinsic compliance. This makes them well suited for the actuation of kinematic redundant manipulators, but due to limited deflection of the muscles and highly nonlinear static and dynamic characteristics, new challenges arises.**

In this contribution, redundancy resolution and control strategies are presented, which take the main actuator nonlinearities into account to make effective use of the advantages provided by the pneumatic muscle actuators. The presented approach is demonstrated on a manipulator consisting of modular segments each actuated by a pair of pneumatic muscle actuators. The approach proves to allow the avoidance of the pressure- and deflection-dependent joint limits to ensure maximum controllability of the manipulator at each point in the workspace.

I. Introduction

Pneumatic actuation provides a number of favorable properties especially well suited to the design of manipulators working in an obstructed environment: their high force-to-weight ratio [1] allows to combine a larger number of segments in a light-weight structure to feasibly realize manipulators with a high degree of redundancy [2], [3], increasing the movability in the presence of obstacles. Furthermore, as all possible measures have to be taken to avoid damage to the manipulator and the environment by unexpected contact, the inherent compliance of fluidically driven manipulators provides an important intrinsic safety feature to complement the use of collision avoidance and detection algorithms in the control structure [4], [5].

Pneumatic artificial muscles (PAM) feature lightweight and compact design, in combination with the obtainable high forces and an intrinsic compliance. This makes them a suitable choice for the actuation of manipulators, but due to the multitude of nonlinear effects and the limited contraction, pneumatic muscles have only been used in a small number of academic applications so far.

Siciliano presents important principles for the redundancy resolution of kinematically redundant manipulators in his 1990 survey [6]. Since then, a multitude of application specific redundancy resolution approaches have been suggested, focusing on the exploitation of the kinematic redundancy to improve task execution [7], [8]. The suggested approaches did not yet allow to take actor nonlinearities into account, as they were developed without regard for the type of actuator used. When using pneumatic muscle actuators in kinetic redundant manipulators a new set of challenges arises, due to limited deflection of the single muscles and highly nonlinear static and dynamic characteristics. In this contribution, redundancy resolution and control strategies are presented, which take the main actuator nonlinearities into account to make use of the advantages provided by the pneumatic muscle actuators.

M. Calabria, F. Schreiber, Y. Sklyarenko and W. Schumacher are with the Institute of Control Engineering, Technische Universität Braunschweig, 38106 Braunschweig, Germany.

A. Raatz is with the Institute of Machine Tools and Production Technology, Technische Universität Braunschweig, 38106 Braunschweig, Germany.

D. Inkermann and T. Vietor are with the Institute for Engineering Design, Technische Universität Braunschweig, 38106 Braunschweig, Germany.

Corresponding author: calabria@ifr.ing.tu-bs.de

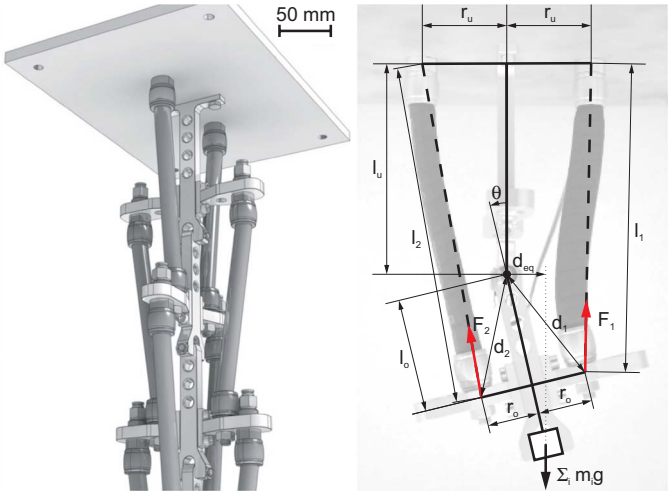

Fig. 1. Manipulator structure and kinematic relations on a single segment.

The approach is demonstrated for the modular structure depicted in Fig. 1, consisting of identical manipulator segments, as presented in [3]. Each of the segments is actuated by an antagonistic pair of pneumatic muscles (FESTO DMSP type, nominal length 150 mm, diameter 10 mm).

In order to visualize the results, the approach is demonstrated on a structure made up by six segments, each with one degree of freedom (DOF), controlled in two translational degrees of freedom at the end-effector, thus dealing with four redundant DOF in the structure.

II. Redundancy resolution scheme

When the number of drives in a manipulator structure exceeds the number of degrees of freedom necessary for a specific task, the structure is said to possess redundant degrees of freedom. For a serial manipulator, the direct kinematic problem that relates the joint positions $\mathbf{q}$ to the pose

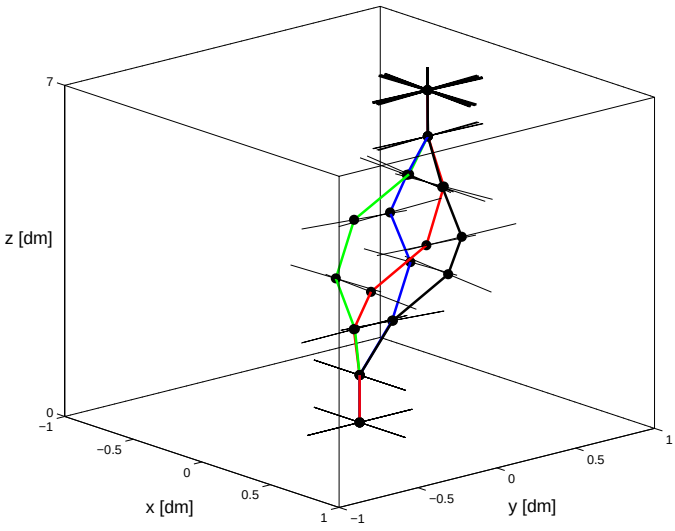

Fig. 2. Different configurations of the kinematically redundant manipulator leading to the same pose of the end-effector.

of the end-effector $\mathbf{x}$ has a finite number of solutions, most of which are trivial. However, the inverse mapping is not uniquely defined for kinematically redundant manipulators, since an infinite set of possible joint configurations $\mathbf{q}$ can be found, that result in the same pose of the end-effector $\mathbf{x}$. An example is shown in Fig. 2.

Because no closed-form solution exists, the inverse kinematic problem can only be solved numerically. In order to choose one of the infinite number of possible solutions, additional tasks or performance criteria has to be defined. For a redundant manipulator actuated by pneumatic muscles joint limits have to be taken into account, since the muscles' range of deflection is restricted. With the maximal contraction ratio of 25% and the geometric properties of the structure, this leads to a controllable joint angle range of $-30^\circ \leq q_i \leq +30^\circ$. One important issue when calculating the joint angles from the set of solutions of the inverse kinematic problem is, therefore, to keep them as small as possible, e.g. by looking for a solution that minimizes the cost function $J = \mathbf{q}^T\mathbf{q}$. A simple optimization for small joint angles over the whole structure may still lead to solutions in which single angles exceed the admissible joint limits. In Fig. 4 (solid lines) the solution of the inverse kinematic problem for a given end-effector path is shown. This path is defined in two DOF in Cartesian space, consequently providing the six joint manipulator with four redundant DOF. The minimization of the joint angles for a given pose leads to solutions in which the cost function $J = \mathbf{q}^T\mathbf{q}$ is minimal and most of the joint angles are quite small at the expense of the angle shown in red, to an extent that it becomes larger than the largest possible angle θ_{max}.Therefore, the joint limits mentioned above also need to be taken into account in the redundancy resolution scheme. A proposed weighting function which allows to minimize joint angles while regarding joint limits is the so-called *logarithmic barrier* [9], which can be expressed as follows:

$$f(\mathbf{q}) = \sum_i \left(\frac{q_i}{q_{i_{max}}}\right)^2 - \ln\left(1 - \left(\frac{q_i}{q_{i_{max}}}\right)^2\right). \quad (1)$$

The weight grows towards infinity as the angle approaches the joint limits. Therefore, joint angles growing towards the limits will be severely punished. The shape of the weight function is shown in Fig. 3.

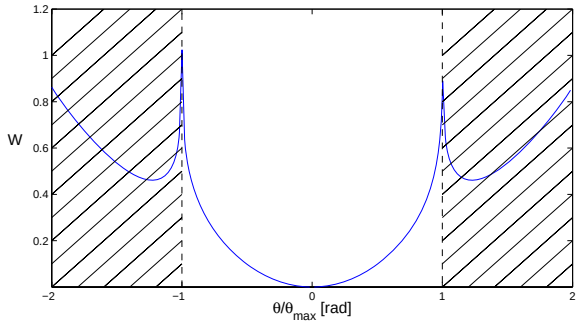

Fig. 3. Weighting function over the admissible angle range.

The search for an optimal joint vector $\mathbf{q}$ that minimizes the cost function (1) under the constraint $\mathbf{x} = \mathbf{g}(\mathbf{q})$ is conducted via convex optimization. This task is a type of constraint minimization problem that can be solved using Lagrange multipliers λ. To combine both constraints into one equation, the following Lagrangian function can be used:

$$\Lambda(\mathbf{q}, \lambda) = f(\mathbf{q}) + \lambda^T(\mathbf{g}(\mathbf{q}) - \mathbf{x}), \quad (2)$$

with the unknown row vector λ^T, which defines a linear combination of the constraints. A local extremum of the Lagrangian function can be found using a gradient descent approach:

$$\nabla\Lambda(\mathbf{q}, \lambda) = 0. \quad (3)$$

An effective strategy to solve the resulting nonlinear system of equations is the Newton-Raphson-method, where the zeros $\mathbf{X}$ of the system $\mathbf{F}(\mathbf{X}) = 0$ are calculated through the following linear iteration formulas:

$$J_\mathbf{F}(\mathbf{X}^p)\Delta\mathbf{X}^p + \mathbf{F}(\mathbf{X}^p) = 0, \quad (4)$$

$$\mathbf{X}^{p+1} = \mathbf{X}^p + \Delta\mathbf{X}^p. \quad (5)$$

Starting from vector $\mathbf{X}^0$, the vectors $\mathbf{X}^{p+1}$ are iterated until the absolute value of the change of the solution vector is smaller than the stopping criteria ϵ. The system of equations in (3) can be split into two parts, one for the vector $\mathbf{q}$, the other for λ: $\mathbf{X} = \begin{bmatrix}\mathbf{q}^T & \lambda^T\end{bmatrix}^T$.

$$\mathbf{F} = \begin{bmatrix}\mathbf{F_1}\\ \mathbf{F_2}\end{bmatrix} = \begin{bmatrix}\frac{\partial}{\partial\mathbf{q}}\Lambda(\mathbf{q},\lambda)\\ \frac{\partial}{\partial\lambda}\Lambda(\mathbf{q},\lambda)\end{bmatrix} = \begin{bmatrix}\nabla f(\mathbf{q}) + J_g^T(\mathbf{q})\lambda\\ g(\mathbf{q}) - \mathbf{x}\end{bmatrix}. \quad (6)$$

The first part is responsible for the optimization and the second for the constraints. Both parts can be solved using the Newton-Raphson-method. The only difficulty is to calculate

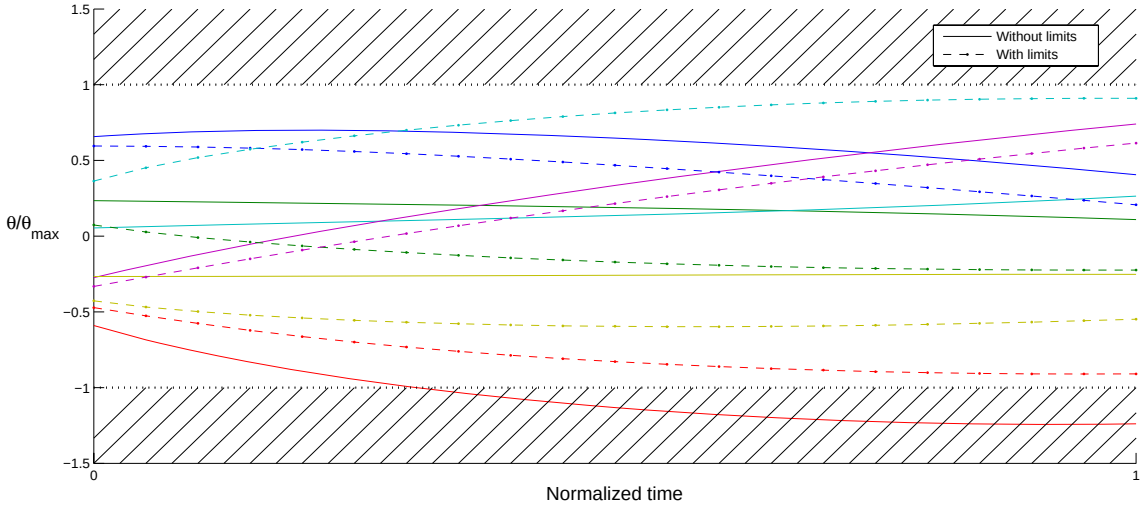

Fig. 4. Planned trajectories for the manipulator joint angles resulting from an unweighted minimization of the joint angles (solid lines) and a minimization of the weighted angles (dashed).

the Jacobian. Equation (7) represents the linear system that has to be solved. $\mathbf{J}_1$ and $\mathbf{J}_2$ are the Jacobians of $\mathbf{F_1}$ and $\mathbf{F_2}$.

$$\begin{bmatrix} \mathbf{J}_1(\mathbf{q},\lambda) \\ \mathbf{J}_2(\mathbf{q}) \end{bmatrix} \begin{bmatrix} \Delta\mathbf{q} \\ \Delta\lambda \end{bmatrix} = - \begin{bmatrix} \mathbf{F_1}(\mathbf{q},\lambda) \\ \mathbf{F_2}(\mathbf{q}) \end{bmatrix}. \tag{7}$$

To calculate the Jacobian matrix $\mathbf{J}_1$, it can be first written as two separate matrices:

$$\mathbf{J}_1 = [\mathbf{J}_{1,1}, \mathbf{J}_{1,2}] = \left[\frac{\partial}{\partial \mathbf{q}} \mathbf{F_1} \ , \ \frac{\partial}{\partial \lambda} \mathbf{F_2} \right]. \tag{8}$$

Both submatrices $\mathbf{J}_{1,1}$ and $\mathbf{J}_{1,2}$ are derived through inspection of equation (6):

$$\mathbf{J}_{1,1} = \frac{\partial}{\partial q_j} \frac{\partial}{\partial q_i} \left(f(\mathbf{q}) + \lambda^T g(\mathbf{q}) \right). \tag{9}$$

The same approach for $\mathbf{J}_2$ results in

$$\mathbf{J}_2 = [\mathbf{J}_g(\mathbf{q}) \ , \ 0]. \tag{10}$$

With these matrices, the iteration formulation is at hand:

$$\begin{bmatrix} \mathbf{q}^{p+1} \\ \lambda^{p+1} \end{bmatrix} = \begin{bmatrix} \mathbf{q}^{p} \\ \lambda^{p} \end{bmatrix} - \begin{bmatrix} \mathbf{J}_{1,1}^{p} & \mathbf{J}_{g}^{p^T} \\ \mathbf{J}_{g}^{p} & 0 \end{bmatrix}^{-1} \begin{bmatrix} \mathbf{F_1}^{p} \\ \mathbf{F_2}^{p} \end{bmatrix}. \tag{11}$$

Fig. 4 shows two inverse kinematics solutions for a movement of the end-effector of a six DOF manipulator along a path defined in two DOF in Cartesian space. The kinematic redundancy is resolved to find consistent joint trajectories that minimize the specific cost functions. Shown in solid lines are the manipulator joint angles resulting from unweighted minimization (solid lines). This simple minimization still allows a violation of the joint limits, happening for the angle shown in red. The minimization of the angles weighted with (1) is shown in dashed lines. As it can be seen, the use of the weight function ensures the compliance of the planned trajectories with the joint limits.

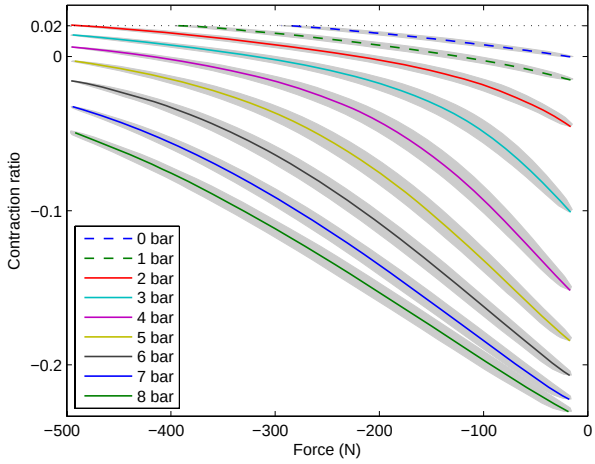

Fig. 5. Load force and contraction curves for an isobarically loaded pneumatic muscle of type FESTO DMSP-10-150N.

III. Joint Limit Estimation

So far, an optimal solution for the inverse kinematic problem has been found based on the premise that the angle in each joint stays as small as possible, avoiding joint limits. Nonetheless, these limits were supposed to be static and equal for each joint. This is not the case on a muscle actuated manipulator, where the maximal contraction is related to the force it exerts.

The relationship between muscle contraction and force can be measured under isobaric conditions, as shown in Fig. 5. The gray areas shown are related to the hysteretic behavior of the muscles, while the lines represent their averages. These lines are limited by the working area of the muscle.

The force that a muscle and its symmetric counterpart must exert to bring the end effector to the desired pose

is related to the position of the joints in space, since th net torque resulting of the action of a pair of antagonist muscles must equal the equivalent torque exerted by gravit on the manipulator. The diagram in Fig. 1 represents th actuating forces on the first segment when the manipulat reaches a static position. The shaded box represents th following segments as a lumped element of weight mg ar an equivalent center of mass. The latest can be calculated a a function of the joint vector $\mathbf{q}$ and the geometric propertie of the structure. With this into account, the following stat equation is obtained by inspection:

$$F_1\, d_1 - F_2\, d_2 = m\, g\, d_{eq}, \tag{1}$$

being d_1 and d_2 geometric functions of the joint ang θ. Since the structure is symmetric, both functions can be resumed into a single one, namely $d(\theta)$, with $d_1 = d(\theta)$ and $d_2 = d(-\theta)$. This function can be derived as the minimum distance between the center of the joint and the line depicted by the muscle, which can be written using vector algebra as

$$d(\theta) = \frac{\mathbf{v^T}}{|\mathbf{v}|} \cdot \begin{pmatrix} r_u \\ l_u \end{pmatrix}, \tag{13}$$

with $\mathbf{v}$ is a vector perpendicular to the muscle:

$$\mathbf{v}(\theta) = \begin{pmatrix} l_u \\ -r_u \end{pmatrix} + \begin{pmatrix} \cos\theta & -\sin\theta \\ \sin\theta & \cos\theta \end{pmatrix} \begin{pmatrix} l_0 \\ r_0 \end{pmatrix}. \tag{14}$$

Further geometric analysis of the structure yields a relationship between joint angle and muscle length l, which leads to

$$l(\theta) = \left| \begin{pmatrix} r_u \\ l_u \end{pmatrix} + \begin{pmatrix} \cos\theta & -\sin\theta \\ \sin\theta & \cos\theta \end{pmatrix} \begin{pmatrix} -r_0 \\ l_0 \end{pmatrix} \right|. \tag{15}$$

Based on symmetry, both muscle lengths can be related to this function, namely $l_1 = l(\theta)$ and $l_2 = l(-\theta)$.

Applying the relationships derived in Eq (13) and (15) to the measured data displayed in Fig. 5, a characteristic surface Φ can be derived, as shown in Fig. 6. This surface illustrates the correspondence between exerted torque, joint angle and pressure, while its domain is restricted by the working area of the pneumatic muscle. These restrictions are of interest, since they determine indirectly the joint limits.

Intersecting this restricted surface with the plane of constant θ produces a segment of line relating air pressure and torque, which can be expressed as

$$\tau = \tau_\theta(P). \tag{16}$$

A second segment is obtained for the antagonistic muscle as well, replacing the angle with its negative. This two segments can be plotted together as in Fig. 7. Infinite combinations satisfying Eq. (12) can be found, so that $\tau_\theta - \tau_{-\theta} = mgd_{eq}$. The selected pair is the one that compromises minimal air pressure.

The torques of each muscle can be determined in Fig. 7 as well, projecting the marked points into the torque axis. This value can be used to calculate joint limits, by looking at the working area of the muscles actuating the joint.

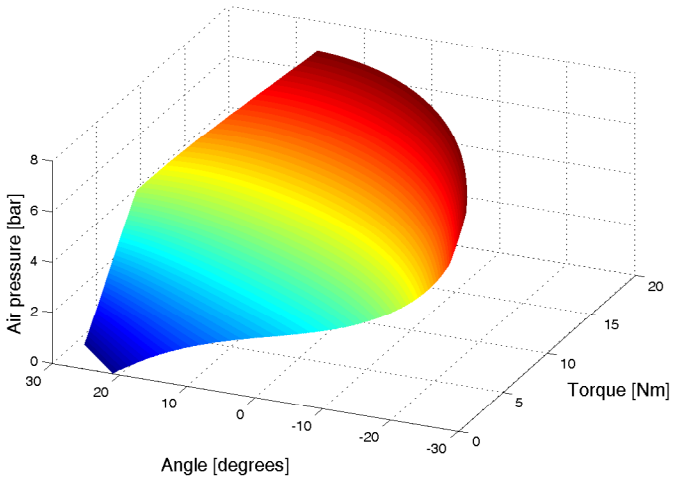

Fig. 6. Characteristic surface of a muscle considered as a torque actuator.

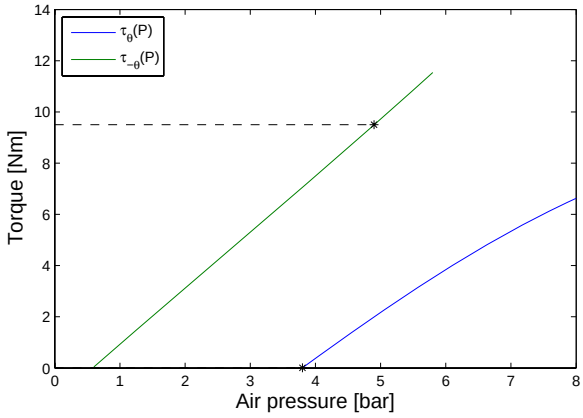

Fig. 7. Torques as a function of pressure P for a given angle θ.

The projection of the characteristic surface Φ into the torque-angle plane is shown in Fig. 8. The feasible joint angles can be computed for both muscles evaluating the working area for the given torques, as highlighted by the dot-dash line. The absolute value of the smallest of the limits, indicated in the figure with a blue line, is the resulting joint limit.

Approximating the characteristic surface with a polynomial function and operating accordingly, a closed mathematical function ξ can be found, such that

$$\mathbf{q}_{max} = \xi(\mathbf{q}). \tag{17}$$

IV. Numerical Implementation

A solution to the inverse kinematic problem was introduced in section II. With this approach, an optimal vector in joint space can be computed numerically, as a function of joint limits and an underdetermined pose in Cartesian space. In section III, a method to evaluate joint limits as a function of the joint vector was described. Nevertheless, both problems should be solved simultaneously in order to ensure optimality and conformance to feasible joint angles.

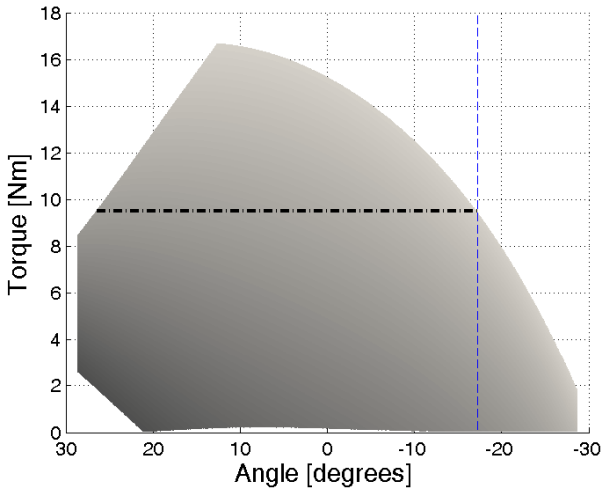

Fig. 8. Working area of the actuated joint and derived joint limit.

A first approach to solving both problems together would be to replace joint limits in Eq. (1) with the closed function (17), and continue to solve the inverse kinematics numerically. Nonetheless, the matrices in (11) result in an ill-posed system even after regularization, and consequently cannot be solved with current processors. This situation also renders other quasi-Newton methods unusable. On the other hand, replacing the limits without recomputing the iteration Jacobians yields a highly numerically unstable system, which requires the implementation of an update method [10].

A means of dealing with this issue is the use of a continuation method, employing a parameter to move from a problem with an easily determined solution to that of the original nonlinear problem. A new problem is therefore defined, namely the resolution of

$$\mathbf{G}(\alpha, (\mathbf{q})) = \nabla\Lambda(\mathbf{q}, \lambda) - (1-\alpha)\nabla\Lambda(\mathbf{q}_0, \lambda_0) = 0, \quad (18)$$

solving iteratively for values of α increasing from 0 to 1, and starting from a known solution $\mathbf{q}_0, \lambda_0$. It can be seen that, for $\alpha = 0$, the system adopts the trivial solution $\mathbf{q} = \mathbf{q}_0$, while the staring vector vanishes for $\alpha = 1$. After each iteration, the values of the limits are updated, and the Lagrange function is solved numerically. This method provides for the simultaneous resolution of Eq. (3) and (17), and its stability is assured by the Homotopy Convergence Theorem [11].

Fig. 9 shows the results of the complete algorithm for the first joint of the manipulator. This joint is generally the one that must exert the highest torque, since its axis is parallel to gravity. Therefore it can be seen that the limit decreases as the joint angle gets larger and the manipulator's center of mass moves farther away from its rest position.

V. Proposed Controller

Appropriate control structures for pneumatic actuators in motion control has been a topic of recent studies. Although different approaches have been investigated [12], [13], most

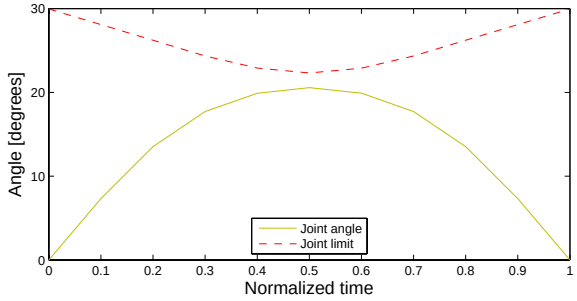

Fig. 9. First-joint value and limit for a given motion in space.

difficulties revolve around the absence of a global dynamic model. In our case, the problem is aggravated, since the goal is to control a set of joints actuated indirectly by antagonistic pneumatic muscles. To simplify the task we will focus on a single joint as in Fig. 1, controlling its angle by adjusting air pressure in two muscles. Each muscle is actuated by an electronic pressure valve, whose time constant is depreciable. Even though no dynamics are specified for this plant, it can be assured that it possesses no pure integrators, since the joint angles are function of the contraction ratio of the muscles only. Therefore, a simple approach to controlling joint angles is to implement a PI controller, given its robustness and asymptotic tracking capabilities of constant input.

A biasing pressure must be added to the output of the controller, since the muscles can only contract when the pressure in their interior is higher than the atmospheric pressure. Nonetheless, biasing the muscle with half the nominal pressure forces an unnecessarily large pretension, hence reducing the maximal torque difference, while using a different value yields to saturation problems. A different approach to this issue is to feedforward a workspace-dependent air pressure. This leaves the controller with the only task to compensate disturbances and model uncertainties, hence increasing the dynamic response. Feedforward values can be obtained out of the evaluation of the characteristic surface done for the redundant resolution of the inverse kinematics.

Further inspection of the surface Φ gives rise to a second control strategy. The values obtained by differentiating the pressure with respect to joint angle and evaluating it at the working point can be used as a variable gain in the control loop, which causes two positive effects. In the first place, varying the gain of a PI controller varies the controller itself, normalizing indirectly its output for different states of the muscles. On the other hand, it accounts for asymmetry in the actuators, since the increment in pressure needed to contract the muscle an extra 1% is larger than the decrement needed to let the muscle stretch that same 1%.

Finally, the transport delay is measured in the pneumatic system and integrated in the controller. A block diagram including the proposed controller can be seen in Fig. 10 and a set of step responses is shown in Fig. 11, for both the proposed controller and the biased complementary PI controller.

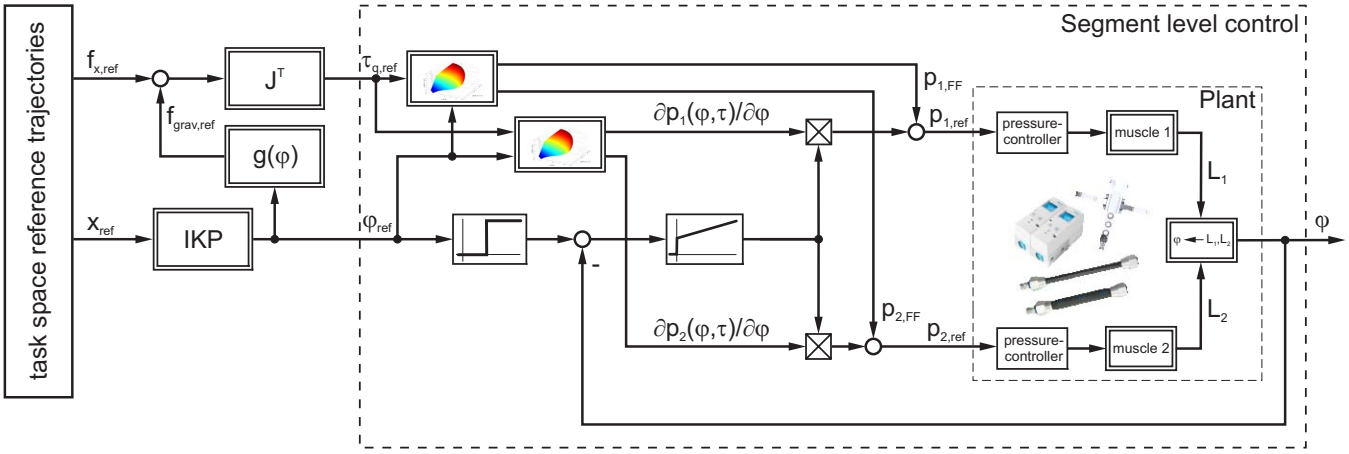

Fig. 10. Block diagram of the closed loop system with position control.

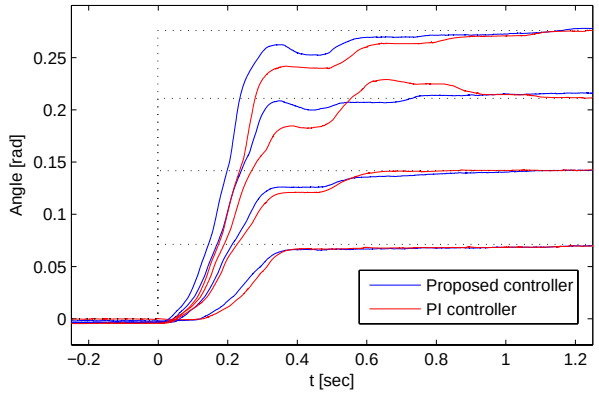

Fig. 11. Angle step response for different reference signals.

VI. Conclusion

Due to their limited deflection and static nonlinear characteristics, pneumatic artificial muscles have not gained widespread application in manipulator motion control. Although the obtainable high forces and low weight of those pneumatic muscles lend themselves to the actuation of highly segmented manipulator structures, the inherent nonlinearities of the pneumatic actuator have prevented their use so far.

In order to obtain feasible control results when actuating kinematic redundant manipulators, the dominant nonlinear muscle characteristics have to be taken into account in the redundancy resolution phase. In this work, an algorithm is presented to transform the nonlinear longitudinal muscle characteristics into the corresponding relation at the joint level of an antagonistically actuated, segmented manipulator. It is shown how this can be used to predict the variable joint limits from the nonlinear muscle characteristics and how these can in turn be taken into account in the redundancy resolution process. This step ensures the calculation of joint level trajectories, that allow a maximal controllability in spite of the actuator nonlinearities.

As the nonlinear mapping on the joint level has been derived, a control structure is presented which exploits this knowledge to compensate the manipulators nonlinearities by an adaptive gain-scheduling approach.

References

[1] J. M. Hollerbach, I. W. Hunter, and J. Ballantyne, *A comparative analysis of actuator technologies for robotics*. Cambridge, MA, USA: MIT Press, 1992, ch. 11, pp. 299–342.

[2] B. Tondu, S. Ippolito, J. Guiochet, and A. Daidie, "A seven-degrees-of-freedom robot-arm driven by pneumatic artificial muscles for humanoid robots," *Int. J. Rob. Res.*, vol. 24, pp. 257–274, April 2005.

[3] J. Schmitt, F. Grabert, and A. Raatz, "Design of a hyper-flexible assembly robot using artificial muscles," in *Robotics and Biomimetics (ROBIO), 2010 IEEE International Conference on*, dec. 2010, pp. 897 –902.

[4] O. Ivlev, S. Schulz, U. Brenk, R. Resinger, G. Dietz, and B. Böhm, "Verbundprojekt PORTASOR - Neue Generation von portablen Soft-Roboterarmen mit sanften Greifern auf Basis von elastischen fluidischen Gelenken für alltägliche Assistenz- und Serviceaufgaben," 2006-2010.

[5] A. Albu-Schäffer, O. Eiberger, M. Grebenstein, S. Haddadin, C. Ott, T. Wimböck, S. Wolf, and G. Hirzinger, "Soft robotics - from torque feedback-controlled lightweight robots to intrinsically compliant systems," *Robotics Automation Magazine, IEEE*, vol. 15, no. 3, pp. 20–30, 2008.

[6] B. Siciliano, "Kinematic control of redundant robot manipulators: a tutorial," *Journal of Intelligent & Robotic Systems*, vol. 3, no. 3, pp. 201–212., 1990.

[7] G. Schreiber, "Steuerung für redundante Robotersysteme: Benutzer- und aufgabenorientierte Verwendung der Redundanz," Ph.D. dissertation, Institut für Robotik und Mechatronik, DLR, 2004.

[8] R. V. Patel and F. Shadpey, *Control of Redundant Robot Manipulators: Theory and Experiments*, 1^{st} ed., ser. Lecture Notes in Control and Information Sciences. Springer Berlin, 2005.

[9] S. Boyd and L. Vandenberghe, *Convex optimization*. Cambridge University Press, 2004.

[10] E. Allgower and K. Georg, *Introduction to numerical continuation methods*, ser. Classics in applied mathematics. Society for Industrial and Applied Mathematics, 2003.

[11] R. Burden and J. Faires, *Numerical Analysis*. Cengage Learning, 2010.

[12] I. Boblan, R. Bannasch, A. Schulz, and H. Schwenk, "A human-like robot torso ZAR5 with fluidic muscles: Toward a common platform for embodied AI," in *50 Years of Artificial Intelligence*, ser. Lecture Notes in Computer Science, M. Lungarella, F. Iida, J. Bongard, and R. Pfeifer, Eds. Springer Berlin / Heidelberg, 2007, vol. 4850, pp. 347–357.

[13] D. Schindele and H. Aschemann, "Disturbance compensation strategies for a high-speed linear axis driven by pneumatic muscles," in *Proceedings of the European Control Conference 2009*, August 2009, pp. 436–441.